Proc. 18th Winter Workshop on Nuclear Dynamics (2002) 000–000

18th Winter Workshop on Nuclear Dynamics
Nassau, Bahamas
January 20–27, 2002

Heavy Flavor Physics in PHENIX

Kenneth N. Barish for the PHENIX Collaboration

Department of Physics
University of California at Riverside,
Riverside, CA 92521

Abstract. Measurement of heavy flavor in heavy ion collisions is sensitive to the initial gluon density and the formation of a deconfined state. The PHENIX detector at RHIC is well designed to study heavy flavor physics in heavy ion collisions. This physics program has begun with the measurement of the single electron spectra in Au+Au collisions at $\sqrt{s_{NN}} = 130\,GeV$. This paper reports on the heavy flavor physics program in PHENIX, the first measurement from Year-1 data and its implication for charm production from the first year of RHIC running, and the prospects for the second year of RHIC running.

Keywords: PHENIX, charm, RHIC
PACS: 25.75.Dw

1. Introduction

The measurement of states involving charm and bottom quarks are rich in physics as they are sensitive to various states of heavy-ion reactions. In the earliest part of the collisions, heavy flavor states such as quarkonium, open charm, and open bottom are dominated by gluon-gluon fusion (e.g. $gg \rightarrow c\bar{c}$). Their production is, thus, sensitive to the initial gluon density [1, 2]. In the presence of a dense plasma, it is been suggested that heavy quark bound states such as the J/ψ will be disassociated due to color screening and the presence of high momentum gluons, leading to their suppression [3]. Meanwhile, heavy quarks may suffer energy loss through gluon radiation in a dense plasma [4] in a similar manner as light quarks [5, 6], although the finite velocity of heavy quarks will suppress this effect [7]. Finally, heavy-quark states can be produced thermally at the very high temperatures that are possible during the plasma state.

This rich set of physics can only be decomposed with a comprehensive set of measurements in $p+p$, $p+A$, and $A+A$ collisions in a variety of channels and kinematic regions. The PHENIX detector's high rate, trigger, and lepton identification capabilities are well matched to this physics. This program has begun with the measurement of the sin-

ISBN 963 00 0000 0

gle electron transverse momentum spectra from the first year of RHIC running of Au+Au at $\sqrt{s_{NN}} = 130\ GeV$ [8]. The second year of RHIC running will allow for the first look at quarkonium and correlated di-leptons as well as a high-statistics single electron measurement.

2. Heavy Flavor Physics in Heavy Ions

PHENIX can measure quarkonium states through their lepton decays (e.g. J/ψ into e^+e^- and $\mu^+\mu^-$). Direct reconstruction of open charm (e.g. $D^0 \to K^-\pi^+$) is ideal, while reconstruction via displaced vertices (e.g. $D \to eX$) may be ultimately possible with upgrades [9]. However, the lepton identification capabilities of the current PHENIX detector also allow for an excellent measurement of open charm and bottom contributions through single leptons and correlated lepton pairs. For example, $D^0 \to K^-l^+\nu_l$ and $\overline{D^0} \to K^+l^-\overline{\nu_l}$, so that $c\overline{c} \to D^0\overline{D^0} \to e^+e^-K^+K^-\nu_e\overline{\nu_e}$, $e^-\mu^+K^+K^-\overline{\nu_e}\nu_\mu$, and $\mu^+\mu^-K^+K^-\nu_\mu\overline{\nu_\mu}$. There is a similar set of decays for open bottom. Because these channels have different kinematics, a comprehensive study of the single leptons and correlated lepton pairs can ultimately be used to separate contributions from open charm and bottom.

In addition to heavy-ion collisions, $p+p$ collisions at the same energy is needed to measure the baseline charm cross-section, and $p+A$ collisions is needed to measure the nuclear effects on the gluon and quark structure functions [10].

3. The PHENIX Detector

PHENIX [11] was designed to search for rare signals in an environment with charged particle densities dN/dy $\sim$ 1000. PHENIX was thus designed to have high rate capabilities to search for rare signals such as the J/ψ and Υ, have high granularity to handle the high particle multiplicity environment, and have good mass resolution to be sensitive to changes in the light vector mesons. Due to cost considerations, these requirements are achieved with the sacrifice of acceptance.

The detector consists of two "central" arms which measures electrons, photons, and charged hadrons, and two forward arms to measure muons.

3.1. Central Arms

The PHENIX central arms provide electron, photon, and charged hadron measurements with outstanding resolution over a limited acceptance. The central arms have an acceptance of ± 0.35 units of rapidity and $90°$ in azimuth in each arm. The central detector consists of 2 arms to allow the study of decays with a large Q-value, e.g. $\phi \to e^+e^-$. The placement of the two arms define the transverse momentum reach of the measurements.

The central arms consist of three tracking subsystems: (1) low mass focusing drift chambers designed to have a position resolutions of 150 μm in $r\phi$ and two-track separation of 1.5 mm, (2) non-projective pixel pad chambers designed to give a 3-d position measurements with 3-8 mm space point accuracy, and (3) a time expansion chamber designed

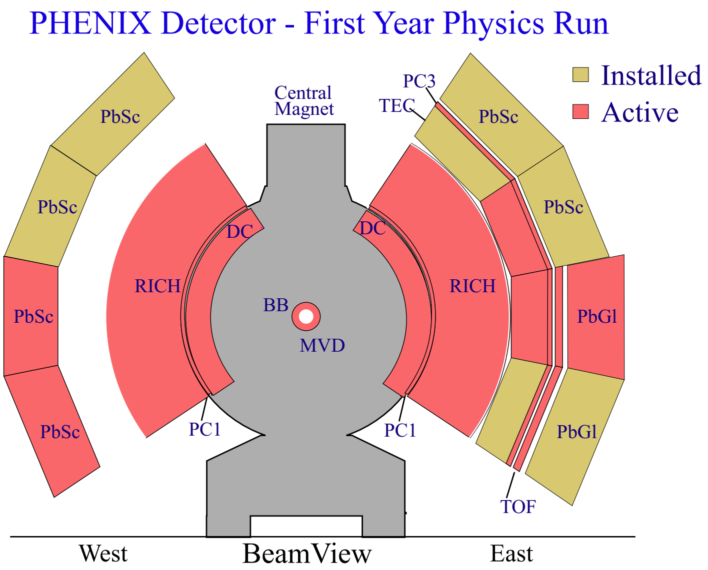

Fig. 1. Installed and active detectors for the RHIC Run-1 configuration of the PHENIX experiment

to give a single point track resolution of 200-250μm in $r\phi$ and a two-track separation of 5 mm. The tracking subsystems is designed to give excellent mass resolution [$\frac{\Delta p_T}{p_t} = 1\%$ at 2 GeV/c, e.g. $\sigma_m(\phi \rightarrow e^+e^-) \approx 4\ MeV$, which is of order of the natural width of the ϕ]

Excellent electron identification is required to reject the large pion multiplicities in heavy-ion collisions. Overall a pion rejection factor of 10^4 up to 6 GeV is achieved with three subsystems: (1) a ring imaging Cerenkov counter which is designed to give a π/e separation of 10^{-4} for $p_t < 4\ GeV/c$ for single pions, (2) a time expansion chamber through dE/dx measurements is designed to provide a rejection of 10^{-2} for P10 gas or 10^{-3} for Xe gas, and (3) an electromagnetic calorimeter designed to yield a rejection of 10^{-2} for $p > 1\ GeV/c$.

3.2. Muons Arms

Each muon arms has a singles acceptance approximately three times that of the central arm, enabling the measurement of the heavy quark bound states with hight statistics and with sufficient mass resolution (e.g. 105 MeV/c^2 for the J/ψ).

Each muon arm covers the full azimuth and has a rapidity coverage of $1.2 \leq |y| \leq 2.5$. Absorber material to shield hadrons is followed by two conical shaped magnets which have a radial field to 4 m. Three stations of cathode strip detectors, $\sigma = 100\mu m$, are followed by muon identification system consisting of 5 gaps filled with Iarocci streamer tubes and 5 layers of steel.

3.3. The PHENIX detector in Year-1

As shown in Fig. 1 the PHENIX central arm detector was partially instrumented for the first year of RHIC data taking, while the muon arms were not in place.

4. PHENIX Year-1 Single Electron Measurement

PHENIX has made the first measurement of the single electron spectra in Au+Au collisions at $\sqrt{s_{NN}} = 130\ GeV$ at RHIC [8].

4.1. PHENIX Electron Identification in Year-1

The measurement of electrons in heavy ion collisions is a challenge, as there are 100–1000 pions for each electron. PHENIX can identify electrons in this environment by (1) determining the momentum from our track reconstruction, (2) finding a matching ring in our Ring Imaging Cerenkov Counter (RICH), (3) matching the momentum from the track with the energy deposited in our Electromagnetic Calorimeter (EMCal), and (4) subtracting random background caused by accidental association of RICH hits with hadron tracks by an event mixing method.

Over 1.2 million minimum bias events were analyzed from Year-1 data and corrected for geometric acceptance, tracking efficiency, and electron identification cuts. The fully corrected transverse momentum spectra is shown in Fig. 2 for central (0-10%), minimum bias (0-92%) and peripheral (60-80%) collisions. The error bars are statistical. The systematic errors are estimated to be 12% at $p_t = 0.5\ GeV$ and 10% at $p_t > 1\ GeV$.

4.2. Light Hadron Contribution to the Electron Spectra

The spectra shown in Fig. 2 includes "background" electrons from decays of light hadrons and their associated photon conversions and Dalitz decays, and "signal" electrons from charm and bottom decay, thermal production, and new physics. In order to study the "signal" we first determine the contributions from the "background".

"Background" electrons come from Dalitz decays of light hadrons (e.g. $\pi^0 \to e^+e^-\gamma$), photon conversions – primarily on the beam pipe and MVD outer shell (e.g. $\pi^0 \to \gamma\gamma \to \gamma e^+e^-$), di-electron decays of light vector mesons (e.g. $\phi \to e^+e^-$), and kaon decays (e.g. $K \to \pi e \nu$).

The electrons from the light hadron decays are estimated from a cocktail calculation that is constrained by PHENIX's pion measurements. The contribution of electrons from photon conversions and Dalitz decays are evaluated using a GEANT simulation of the detector coupled with the hadron decay generator. This is cross checked by comparing the relative yield of reconstructed Dalitz pairs and conversion pairs between the simulation and data, as the p_T spectra from externally converted electrons are almost identical to the spectra from the internally converted Dalitz decays.

The cocktail calculation uses the π spectra from the PHENIX data [6, 12], assuming charge symmetry ($\pi^0 = \pi^+ = \pi^-$) and taking the rapidity to be flat around $y = 0$.

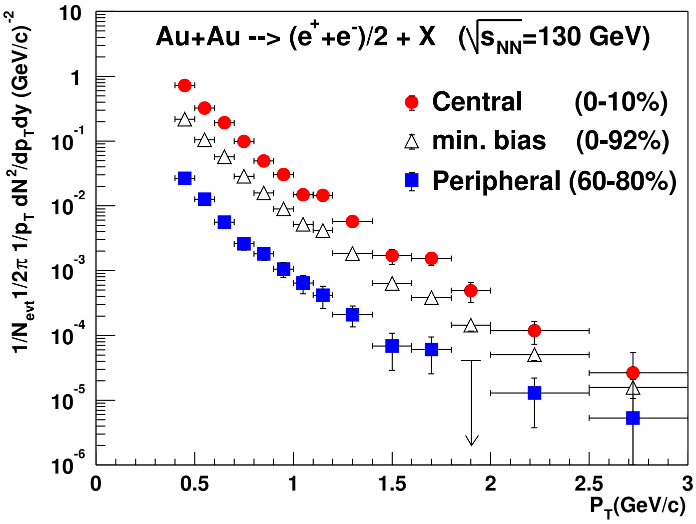

Fig. 2. The transverse momentum spectra of electrons in PHENIX from Au+Au collisions at $\sqrt{s_{NN}} = 130\ GeV$.

M_T scaling, $p_t \rightarrow \sqrt{p_t^2 + m_h^2 - m_\pi^2}$, is used for the other hadrons. The spectra shapes of PHENIX's $p^\pm$ and $K^\pm$ are consistent with this scaling to 20% [12]. At high p_T we take $\eta/\pi^0 = 0.55$, $\eta'/\pi^0 = 0.25$, $\rho/\pi^0 = \omega/\pi^0 = 1.0$ (this is based on proton data from the SPS, FNAL, and ISR [13, 14], SPS data [15]), and $\phi/\pi^0 = 0.4$ (this agrees with the STAR ϕ/h^- inclusive measurement of 0.02 [16]). A 50% systematic error is assigned to these ratios.

The lower pannel of Fig. 3 shows the relative contributions to the background from various sources. 80% of the background is found to be from π^0's, either from Dalitz decays or indirectly through γ conversions.

The upper pannel of Fig. 3 shows the ratio of the electron data to the calculated background as a function of p_T in minimum bias collisions. The shaded band represents the total systematic uncertainties. We see a clear excess above the light hadron cocktail for $p_T > 0.6GeV/c$. The excess increases as a function of p_T, as is expected from a charm contribution. The central data also shows a similar excess, while the peripheral data does not have enough statistics.

The systematic errors in the data and cocktail are roughly equal. The dominant sources of systematic error in the light hadron cocktail come form uncertainties in the normalization and shape of the input π^0 spectrum, the h/π^0 ratios, and the conversion/Dalitz ratio. These systematic errors are minimized by the constraint coming from the PHENIX π data. The dominant sources of systematic error in the data come from uncertainties in the detector efficiency, RICH ID and E/p cut efficiencies, the subtraction of the hadron background, and the EMCal/RICH association.

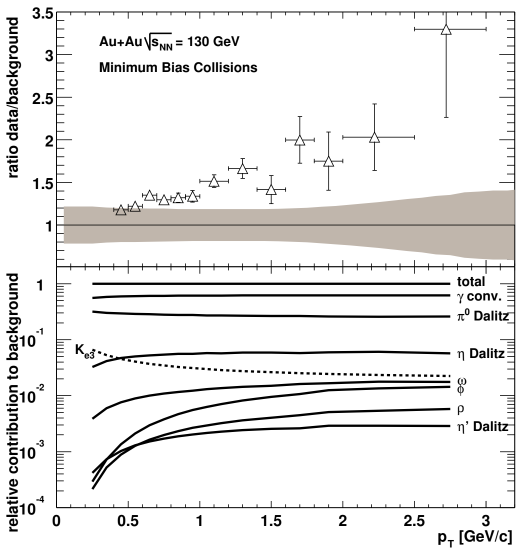

Fig. 3. *Upper pannel:* ratio of electron data to calculated background for minimum bias collisions. *Lower pannel:* relative contributions to the background from various sources.

4.3. Background Subtracted Single Electron Spectra

The background subtracted single electron spectra are shown in Fig. 4. The error bars on the data points represent the statistical errors, while the systematic error due to the background subtraction is indicated by brackets. A clear excess of "signal" electrons is seen.

In order to study the possible charm contribution to the signal, we used a PYTHIA calculation. Default PYTHIA does not reproduce charm production data well at SPS and FNAL [17], and ISR single electron data [18]. Therefore, we tuned PYTHIA to fit these spectra. We used version 6.152, CTEQ5L PDFs, $m_c = 1.25 GeV/c^2$, K=3.5, and $< k_t >= 1.5$. In proton-proton collisions this gives a charm cross section $\sigma_{c\bar{c}} = 330 \mu b$. In the absence of nuclear effects, the electron spectrum in Au+Au collisions is calculated as

$$E\frac{dN_e}{dp^3} = T_{AA} \times E\frac{d\sigma_e}{dp^3}$$

where $Ed\sigma_e/dp^3$ is the production cross section of electrons from charm decays in pp collisions from this PYTHIA calculation, and T_{AA} is the nuclear overlap integral calculated from a Glauber model [6]. The PYTHIA charm calculation is shown as solid lines in Fig. 4. The data is are bit higher than this PYTHIA parameterization. Also shown on the figure is an analogous PYTHIA calculation for bottom decays for central collisions (dashed line), and an prediction for the contribution for direct photons [19].

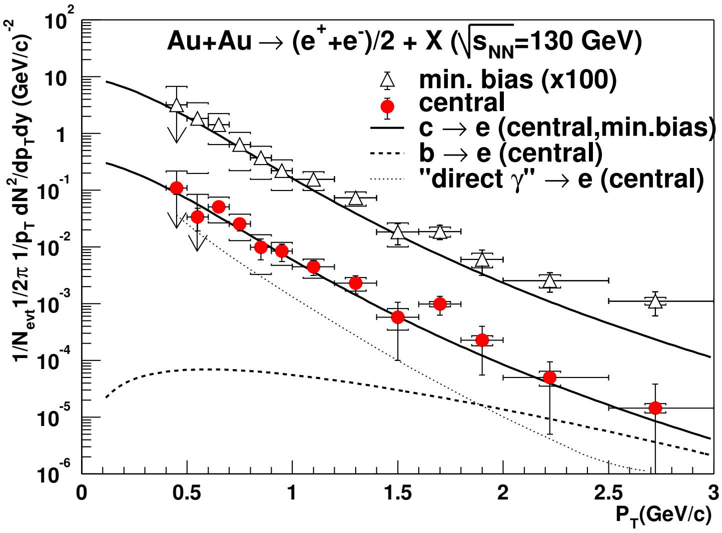

Fig. 4. The background subtracted single electron spectra for minimum bias and central collisions with expected contribution from open charm decays. Also shown are the expected contribution from bottom decays and the a direct photon prediction for central collisions.

4.4. *Implications on the Charm Yield in Heavy-Ion Collisions*

We can estimate the charm yield by assuming that all single electrons above background are from charm. In doing this we neglect other possible sources such as bottom, thermal photons, and di-leptons. These can possibly contribute to the signal in this p_T region by 10-20%, but with large theoretical uncertainties. By fitting the PYTHIA calculation to the data for $p_T > 0.8\ GeV/c$, we obtain charm cross sections per binary NN collisions: $\sigma_{c\bar{c}}^{0-10\%} = 380 \pm 60 \pm 200 \mu b$ and $\sigma_{c\bar{c}}^{0-92\%} 420 \pm 33 \pm 250 \mu b$. The data is consistent with binary scaling, i.e. no nuclear or medium effects, but with large uncertainties. This is an interesting result, as the enhanced di-muon production reported in Pb+Pb collisions at the SPS has been attributed to an increase of charm production [20].

In Fig. 5 we compare the single electron yield signal and the derived charm cross section with the single electron data from ISR experiments and fixed target experiments. The PYTHIA calculations are the ones described earlier in the text. Our data is surprisingly consistent, albeit within large errors, to both the PYTHIA and NLO pQCD [21] calculation.

5. Prospects for Year-2

The prospects for heavy flavor physics results from Year-2 is excellent. During the Year-2 run PHENIX sampled over 170 million $Au + Au$ collisions ($24\ \mu b^{-1}$) at $\sqrt{s_{NN}} = 200 GeV$.

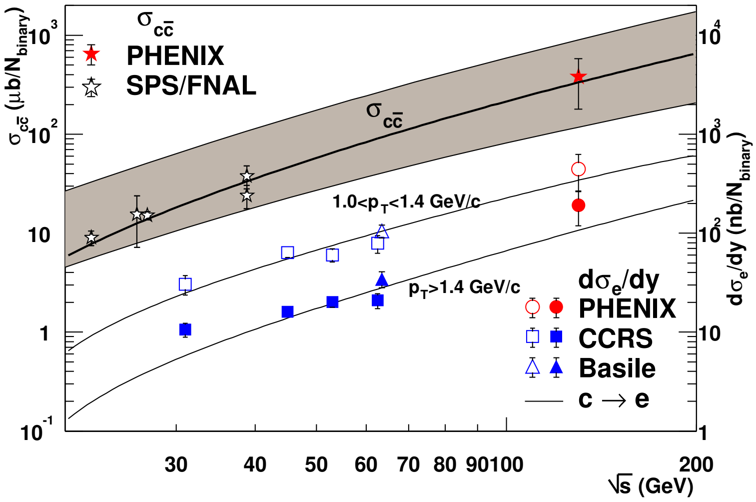

Fig. 5. The single electron cross sections $d\sigma_e/dy$ and charm cross sections $\sigma_{c\bar{c}}$ as a function of energy. The experimental measurements are from this PHENIX measurement, ISR experiments, SPS, and FNAL measurements. The thick curves are calculated with PYTHIA, and the shaded band represents a NLO pQCD calculation.

The PHENIX central arms were fully instrumented and the south muon arm was commissioned. The Level-2 trigger system was also in place, allowing for triggering on single electrons, electron pairs including an invariant mass cut for the J/ψ, single muons, and muon pairs. From this data we expect the first look of $J/\psi \rightarrow e^+e^-$ and $J\psi \rightarrow \mu^+\mu^-$ at RHIC, and an improved single electron spectra. A special "converter" run was taken with heavy ions was conducted to directly measure the background from photon conversion. In addition to the Au+Au run, there was also a $p+p$ from which a baseline charm measurement will me made. We expect that both the systematic and statistical errors of the single electron measurement will be greatly reduced.

6. Conclusion

The PHENIX heavy flavor program has begin. An excess of single electrons above the expected light hadron contribution is seen in the Year-1 data. Neglecting other possible contributions, the excess translates into $\sigma_{c\bar{c}}^{0-10\%} = 380 \pm 60 \pm 200 \mu b$.

Year-2 data will yield a first look at $J/\psi \rightarrow e^+e^-, \mu^+\mu^-$, improved single electron spectra with a special converter run to directly measure the Dalitz/converter contribution, and charm and J/ψ in p+p collisions at 200 GeV.

Acknowledgments

This work is supported by the United States Department of Energy Grant DOE-FG03-86ER40271.

References

1. J.A. Appel, Ann. Rev. Nucl. Part. Sci. **42**, 367 (1992).
2. B. Müller and X.N. Wang, Phys. Rev. Lett. **68**, 2437 (1992).
3. T. Matsui and H. Satz, Phys. Lett. **B178**, 416 (1986).
4. Z.Lin, V. Vogt, X-N. Wang, Phys. Rev. **C57** 899 (1998).
5. M. Gyulassy and M. Plümer, Phys. Lett. **B243**, 432 (1990).
6. K. Adcox *et al.* [PHENIX Collaboration], Phys. Rev. Lett. **88** 022301 (2002).
7. Y. Dokshitzer and D. Kharzeev, Phys. Lett. **B519** 199 (2001).
8. K.Adcox *et al.* [PHENIX Collaboration], submitted to Phys. Rev. Lett. (nucl-ex/0202002).
9. C. Woody *et al.* [PHENIX Collaboration], in these proceedings.
10. K.J. Eskola, V.J. Kolhinen, and R. Vogt, Nucl. Phys. **A696** 729 (2001).
11. D.P. Morrison *et al.* [PHENIX Collaboration], Nucl. Phys. **A638**, 565 (1998).
12. K. Adcox *et al.* [PHENIX Collaboration], submitted to Phys. Rev. Lett. (nucl-ex/0112006).
13. R. Albrecht *et al.,* Phys. Lett. **B361** 14 (1995); G. Agakichiev *et al.*, Eur. Phys. J. **C4**, 249 (1998) and references therin.
14. M. Diakonou *et al.*, Phys. Lett. **B89**, 432 (1980).
15. M. M. Aggarwal *et al.*, nucl-ex/0006007; M. M. Aggarwal *et al.* Phys. Rev. Lett. **85**, 3595 (2000).
16. C. Adler *at al.* [STAR Collaboration], to be published.
17. G. A. Alves *et al.*, Phys. Rev. Lett. **77**, 2388 (1996) and references therin.
18. F.W. Büsser *et al.,* Nucl. Phys. **B113** 189 (1976); P. Perez *et al.*, Phys. Lett. **B112**, 260 (1982); M. Basile *et al.*, Nuovo Cimento **A65**, 421 (1981).
19. J. Alam *et al.*, Phys. Rev. **C63**, 021901 (2001).
20. M. C. Abreu, *et al.*, Eur. Phys. J. **C14**, 443 (2000).
21. M. Mangano, P. Nason, and G. Ridolfi, Nucl. Phys. **B405**, 507 (1993). Their program **HVQMNR** is used with CTEQ5M parton distribution functions to calculate the charm cross section in Fig. 5 with $m_c = 1.5$ GeV/c^2, $\mu_F = 2m_c$, and $0.5m_c < \mu_R < 2m_c$.